Electromagnetically Induced Transparency: Propagation Dynamics

A. Kasapi, Maneesh Jain, G. Y. Yin, and S. E. Harris
Edward L. Ginzton Laboratory, Stanford University, Stanford, California 94305
(Received 23 September 1994)

We describe the temporal and spatial dynamics of propagating electromagnetically induced transparency pulses in an optically thick medium. Results include pulse velocities as slow as $c/165$ with 55% transmission, strong-probe-field effects, and the observation of near diffraction-limited transmitted beam quality.

PACS numbers: 42.50.Gy, 32.80.–t, 42.50.Hz

Electromagnetically induced transparency (EIT) is a process where one laser (or electromagnetic field) is used to modify the absorption coefficient and refractive index seen by a probe laser, thereby allowing it to propagate in what would otherwise be an optically thick medium. Early experimental observations have focused on the total transmission of a weak probe laser [1]. More recent work has focused on such topics as the dispersive properties of EIT [2,3], matched pulse generation [4], normal modes [5], dressed field states [6] and adiabatons [7], spatial consequences of EIT [8], and extensions of these effects to the continuum [9] and to detuned multistate systems [10]. There has also been substantial work on closely related topics such as applications to lasers without inversion [11] and to nonlinear optics [12].

In this work we report the first experimental studies of the temporal dynamics and spatial behavior of propagating EIT pulses. We probe a resonant transition which, without the "coupling" laser applied, has an absorption coefficient of $\alpha = 600/\text{cm}$ over a length of $L = 10$ cm ($\alpha L = 6000$). For a weak probe and strong coupling laser, we observe group velocities as slow as $c/165$ with an energy transmission of 55%. For a strong probe laser we observe reshaping of both the coupling and probe laser pulses and the formation of propagating pulse pairs. Of perhaps most interest, we report the observation of nearly diffraction-limited beam transmission in a medium which, without the coupling laser present, is nearly optically impenetrable.

We work with 99.97% isotopically pure lead (^{208}Pb) vapor in a 10-cm-long sealed fused-silica side-arm cell at a typical density of 2×10^{14} atoms /cm^3. Figure 1 shows the pertinent states and transitions. The probe transition $6s^2 6p^2\,{}^3P_0 \rightarrow 6s^2 6p 7s\,{}^3P_1$ has a wavelength of 283 nm and an oscillator strength of $gf = 0.2$; the coupling laser transition is $6s^2 6p^2\,{}^3P_2 \rightarrow 6s^2 6p 7s\,{}^3P_1$ with a wavelength of 406 nm and $gf = 0.7$ [13].

The 406- and 283-nm laser beams are obtained from independent frequency doubled and tripled Ti:sapphire laser systems operating near 811 and 805 nm, respectively. Each of these systems consists of a continuous-wave external-cavity (Littman configuration) diode laser which seeds a Ti:sapphire ring laser. Each ring laser is pumped with an 8-ns-long pulse at 532 nm from separate commercial yttrium aluminum garnet (YAG) laser systems so that their timing can be independently controlled. The 283-nm system is tuned to the center frequency of the probe transition with an independent Lamb dip cell and is thereafter locked to a temperature-stabilized etalon. The coupling laser is tuned to center frequency by maximizing the EIT effect during the experiment. The coupling and probe lasers have pulse durations of 100 and 12 ns, respectively. At least 99.9% of the output energy of each laser appears in a single longitudinal mode [14]. After frequency doubling and tripling to 406 and 283 nm, the

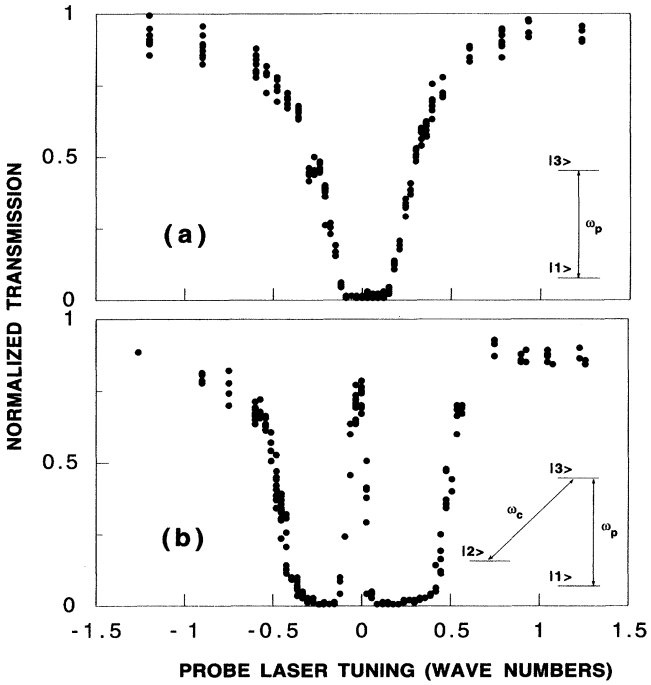

FIG. 1. Transmission vs probe frequency in ^{208}Pb vapor: (a) probe alone ($\Omega_p = 5 \times 10^{-4}$ cm^{-1}, $\Omega_c = 0$) and (b) probe coupling laser ($\Omega_p = 5 \times 10^{-4}$ cm^{-1}, $\Omega_c = 0.4$ cm^{-1}). $|1\rangle$, $|2\rangle$, and $|3\rangle$ denote the states $6s^2 6p^2\,{}^3P_0$ (ground), $6s^2 6p^2\,{}^3P_2$ (metastable), and $6s^2 6p 7s\,{}^3P_1$, respectively. The transmission minimum of the probe alone corresponds to an inferred transmission of e^{-6000}.

0031-9007/95/74(13)/2447(4)$06.00

long-term (one week) stability of each system is under 100 MHz.

The probe and coupling beams have opposite circular polarization and are focused into the center of the cell with beam diameters (measured to the $1/e$ points) of 0.2 and 0.9 mm, respectively. The probe beam is centered on the spatially uniform central portion of the larger coupling laser beam and remains centered for the length of the cell. The relative timing of the two lasers is adjusted so that the coupling laser enters the cell before the probe and is present until after the probe has left the cell. Fast photodetectors connected to a 5×10^9 sample/s Tektronix TDS 684A four-channel, real-time digital oscilloscope and computer simultaneously record the probe and coupling laser pulses before entering (via beam splitters) and after exiting the cell. All data points shown in this Letter are from individual pulses and are not averaged.

The voltage signal of the coupling laser detector is calibrated to the coupling laser Rabi frequency (Ω_c) by fixing the coupling laser power and scanning the probe laser frequency to determine the Autler-Townes splitting of state $|3\rangle$. For good frequency resolution this is done in a relatively optically thin cell. The Rabi frequency of the probe (Ω_p) is not measured directly and is inferred from the $|1\rangle \rightarrow |3\rangle$ transition oscillator strength and the measured power.

Figure 1 shows the probe transmission as a function of the probe wavelength. The probe is sufficiently weak ($\Omega_p < 6 \times 10^{-4}$ cm^{-1}) that there is no saturation. In Fig. 1(a) there is no coupling laser present. From the known transition oscillator strength, cell length, and Lorentzian portion of the linewidth (whose determination is discussed below), we determine the cell density N. For the transmission curve shown, the full-width half-power linewidth is $\gamma_{31} = 1.9 \times 10^8$ rad/s and the atom density is $N = 2 \times 10^{14}$ atoms/cm^3. For a cell of length $L = 10$ cm, this corresponds to an absorption coefficient of $\alpha L = 6000$ for the probe alone and a transmission of $e^{-\alpha L}$.

Figure 1(b) shows the probe transmission as a function of the probe wavelength with the coupling laser present ($\Omega_c = 0.4$ cm^{-1}). Compared with Fig. 1(a), we note that the overall opacity width has increased by about a factor of 2 (optically thick Rabi sidebands) and that there is now an on line center transmission maximum of approximately 90%.

We turn next to the dispersive properties of this system. In the limit of a time-independent and strong coupling laser, a pulse of probe light experiences small loss, unity refractive index, slow group velocity (v_g), and zero group velocity dispersion [2]. Figure 2 shows the first observation of the large propagation delays which are obtainable using EIT. As the Rabi frequency of the coupling laser is decreased, both the loss and the total delay increase. At the smallest coupling laser Rabi

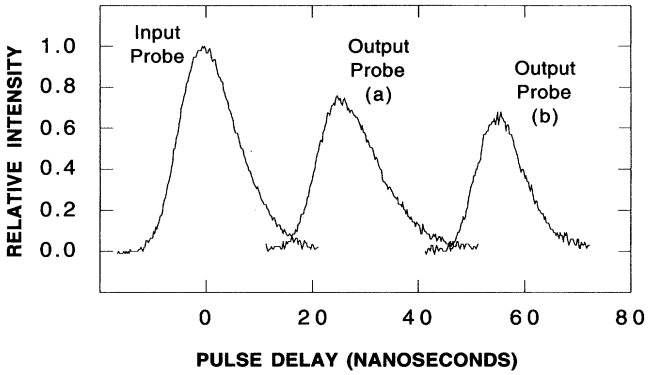

FIG. 2. Transmission vs pulse delay in a 10-cm-long ^{208}Pb cell [$N = (1.6 \times 10^{14}) \pm 30\%$ atoms/cm^3]. The pulse is shown at both the cell input and the cell output. For each pulse the peak probe Rabi frequency is 0.02 cm^{-1}. For pulse (a), as the probe pulse slips through the coupling laser pulse, Ω_c increases from 0.18 to a peak of 0.2 and then falls to 0.18 cm^{-1}. For pulse (b), Ω_c increases from 0.11 to 0.15 and then falls to 0.14 cm^{-1} (i.e., the probe spends most of its time on the rising edge of the coupling laser wave form). Pulse (b) corresponds to a group velocity of $c/v_g = 165$ and 55% energy transmission.

frequency [curve (b)], we observe a probe pulse delay of 55 ns, corresponding to a group velocity normalized to the speed of light of $c/v_g = 165$, and a transmission of 55%. We also observe that the output pulse duration is slightly shorter than the input. This is in contradiction to the linear theory [2] which predicts that higher frequency Fourier components are attenuated, causing the probe pulse to lengthen. We believe that the observed pulse shortening is the result of the time variation of the coupling laser intensity which in turn causes a time-varying group velocity for the probe. In this case, the coupling laser intensity is increasing, so that the instantaneous group velocity of the probe pulse is increasing and the back edge of the probe pulse travels faster than the front edge, causing the pulse to shorten.

By combining the formulas of Ref. [2], it may be shown, for the conditions of this experiment (where Ω_c is larger than the probe Rabi frequency and $\Omega_c \gg \gamma_{31}, \gamma_{21}$), that irrespective of the details of the pulse shape and amplitudes

$$\ln(\mathcal{E}_{\text{out}}/\mathcal{E}_{\text{in}}) = -\gamma_{21}\tau_{\text{delay}}, \qquad \tau_{\text{delay}} = L(1/v_g - 1/c), \tag{1}$$

where $\mathcal{E}_{\text{in}}$ and $\mathcal{E}_{\text{out}}$ are the input and output probe pulse energies, γ_{21} and γ_{31} are the linewidths of the $|1\rangle \rightarrow |2\rangle$ and $|1\rangle \rightarrow |3\rangle$ transitions, respectively, and τ_{delay} is the delay of the probe pulse propagating a distance L through the medium, minus the delay in propagating the same distance in vacuum. This is an important result: The transmission depends only on the linewidth of the $|1\rangle \rightarrow |2\rangle$ transition and on the excess delay of the pulse in the medium. This expression, with γ_{21} replaced by γ_{31},

also holds for a two-state system ($\Omega_c = 0$), where the free parameter is now the detuning of the probe from the $|1\rangle \rightarrow |3\rangle$ transition.

These relations can be interpreted physically. In a medium where a laser pulse propagates with a slow group velocity, most the pulse energy is reactively stored in the medium. In a detuned two-state atomic system [15], the energy is stored as coherent excitation of the $|1\rangle \rightarrow |3\rangle$ transition, and the probe is attenuated because of the dephasing rate of this transition. In an EIT system, the energy is stored as a coherent excitation of the $|1\rangle \rightarrow |2\rangle$ transition, and the probe is attenuated according to its dephasing rate. The maximum obtainable delay for $1/e$ transmission in a two-state system is $1/\gamma_{31}$ and in an EIT system is $1/\gamma_{21}$ [2].

Figure 3, curve (a), combines many single pulses of the type shown in Fig. 2 for many different Rabi frequencies. The x and y axes show the measured delay and natural logarithm of the transmission for each pulse. The data yield a straight line with a slope of 1.0×10^7 rad/s (100 ns lifetime). Figure 3, curve (b), shows the transmission vs excess delay of single probe pulses (no coupling laser) with different detunings. Here, the slope is 1.9×10^8 rad/s (5.2 ns lifetime). Because of the metastability of the $|1\rangle \rightarrow |2\rangle$ transition, the slope of curve (a) is $\frac{1}{19}$ of the slope of curve (b).

In the next set of experiments the Rabi frequency of the probe laser is increased until it is comparable to the coupling laser. Figure 4 shows the probe at the cell input and output and the coupling laser at the cell output. Only the spatial portion of the coupling laser overlapping the probe in the cell is monitored. In Fig. 4(a) we see energy transfer into and then out of the coupling laser pulse, synchronously with the rising and falling edges of the probe laser pulse. In Fig. 4(b), the atom density is increased and the coupling laser intensity decreased. A dip in the coupling laser pulse accompanies the probe laser pulse through the cell. This pulse pair formation is a feature of the adiabatons which have been recently predicted by Grobe, Hioe, and Eberly [7].

We turn next to the spatial properties of strong probe EIT. It is well known [16] that even a beam of saturation intensity will be greatly distorted as it propagates through a resonant optically thick medium. To investigate this effect with our experimental setup, we introduce spatial structure onto the probe beam by passing it through a 2-mm-diameter aperture [17]. The beam then travels 14 cm to a 1-m lens, focuses in the cell, and arrives at a charge coupled device (CCD) camera positioned 200 cm from the lens. Figure 5 shows how EIT allows high quality beam transmission through what would otherwise be an opaque and highly distorting medium. The coupling laser beam acts as a spatial filter for the probe beam. The lowest spatial frequencies of the probe overlap the strongest portions of the coupling laser beam and see nearly perfect transmission and no excess phase shift. Higher spatial frequencies of the probe overlap weaker portions of the coupling laser beam and are somewhat attenauted, so that the beam imaged at the CCD camera is slightly blurred. If the coupling laser is detuned by as little as 200 MHz, the image is distorted, since the spatially varying coupling beam intensity now imposes different phase shifts on the spatial frequencies of the probe beam.

In summary, we have described experimental results showing the temporal and spatial dynamics of EIT in an optically thick medium. At a small probe intensity we observe very slow optical group velocities; at comparable probe and coupling laser intensities we observe the interaction of the probe and coupling laser and the formation of propagating pulse pairs. We also observe

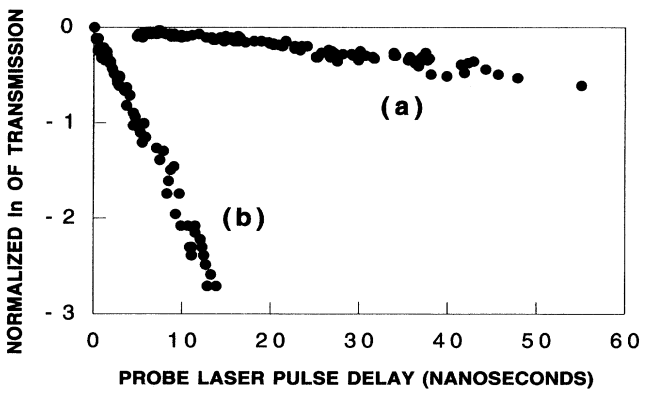

FIG. 3. Natural logarithm of transmission vs probe pulse delay. Many data points from Fig. 2, at different values of Ω_c, are combined to yield curve (a). Curve (b) is obtained with $\Omega_c = 0$ by varying the probe detuning from line center. The slopes of curves (a) and (b) are the linewidths of the $|1\rangle \rightarrow |2\rangle$ and $|1\rangle \rightarrow |3\rangle$ transitions, respectively.

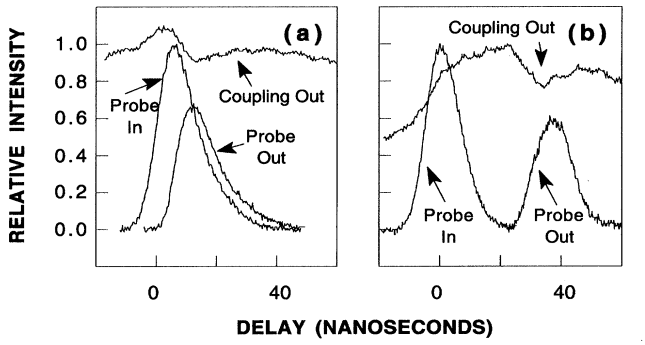

FIG. 4. Normalized transmission vs pulse delay for a strong probe. (a) $\Omega_c = 0.3$ cm^{-1}, $\Omega_p = 0.4$ cm^{-1}, and $N = 6 \times 10^{13}$ atoms/cm^3. Energy is transferred to the coupling laser during the rising edge of the probe pulse and is transferred from the coupling laser during the falling edge of the probe pulse. (b) $\Omega_c = 0.13$ cm^{-1}, $\Omega_p = 0.1$ cm^{-1}, and $N = (1.6 \times 10^{14}) \pm 30\%$ atoms/cm^3. The downward bump on the coupling laser moves at the group velocity of the probe and appears at the output at the same time.

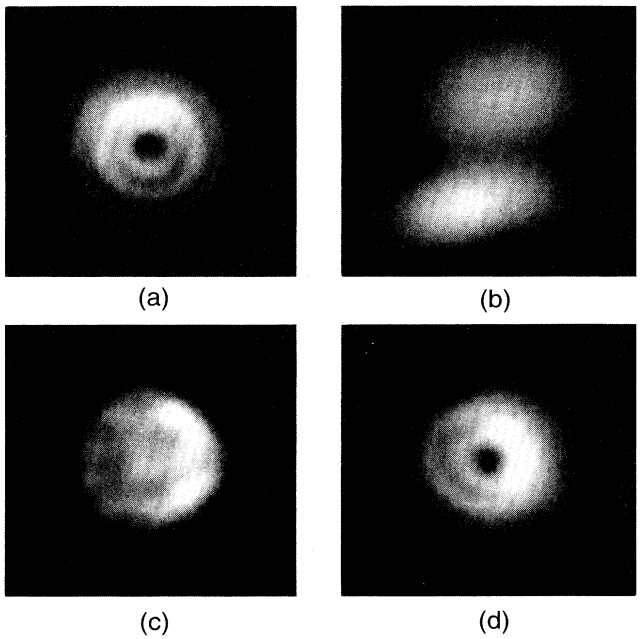

FIG. 5. Spatial images of the probe beam after passage through the Pb cell. (a) Probe alone in a cold cell (note the central dark portion and the faint diffraction rings). (b) Probe alone with a Rabi frequency of 0.5 cm^{-1} (330 kW/cm^2). Here, as in (c) and (d), $N = (1.6 \times 10^{14}) \pm 30\%$ atoms/cm^3. The figure shows a superposition of two probe pulses and is scaled to one-half size to show both images. The beam is spatially distorted and, from shot-to-shot, moves randomly by several beam diameters. (c) Probe and coupling laser with the coupling laser detuned by 200 MHz from line center ($\Omega_p = 0.3$ cm^{-1} and $\Omega_c = 0.8$ cm^{-1}). The transmitted beam is now spatially distorted. (d) Probe and coupling laser with the coupling laser at line center ($\Omega_p = 0.3$ cm^{-1} and $\Omega_c = 0.8$ cm^{-1}). The beam quality is now almost as good as in (a). In order to allow better visibility of the fringe structure, portions of these images are saturated.

near diffraction-limited EIT transmission under conditions where the medium is otherwise highly distorting.

The authors thank A. Merriam, H. Xia, R. Engleman (Opthos Corp.), and L. Hollberg (NIST) for their contributions, and Z. F. Luo, A. E. Siegman, and A. Zibrov (Lebedev Institute) for helpful discussions. The work described here was supported by the U.S. Office of Naval Research, the Army Research Office, and the U.S. Air Force Office of Scientific Research.

[1] K. J. Boller, A. Imamoglu, and S. E. Harris, Phys. Rev. Lett. **66**, 2593 (1991); J. E. Field, K. H. Hahn, and S. E. Harris, Phys. Rev. Lett. **67**, 3062 (1991).
[2] S. E. Harris, J. E. Field, and A. Kasapi, Phys. Rev. A **46**, R29 (1992).
[3] M. Xiao, Y.-Q. Li, S.-Z. Jin, and J. Gea-Banacloche, Phys. Rev. Lett. **74**, 666 (1995).
[4] S. E. Harris, Phys. Rev. Lett. **70**, 552 (1993); G. S. Agarwal, Phys. Rev. Lett. **71**, 1351 (1993); M. Fleischhauer, Phys. Rev. Lett. **72**, 989 (1994).
[5] S. E. Harris, Phys. Rev. Lett. **72**, 52 (1994).
[6] J. H. Eberly, M. L. Pons, and H. R. Haq, Phys. Rev. Lett. **72**, 56 (1994).
[7] R. Grobe, F. T. Hioe, and J. H. Eberly, Phys. Rev. Lett. **73**, 3183 (1994).
[8] R. R. Moseley, S. Shepherd, D. J. Fulton, B. D. Sinclair, and M. H. Dunn, Phys. Rev. Lett. **74**, 670 (1995).
[9] S. J. van Enk, J. Zhang, and P. Lambropoulos, "Coherent Effects through the Continuum: Transparency, Population Trapping and Amplification Without Inversion through Autoionizing Resonances" (to be published).
[10] S. E. Harris, Opt. Lett. **19**, 2018 (1994).
[11] M. O. Scully, Quantum Opt. **6**, 203 (1994), and references therein; O. Kocharovskaya and P. Mandel, Quantum Opt. **6**, 217 (1994).
[12] K. Hakuta, L. Marmet, and B. P. Stoicheff, Phys. Rev. A **45**, 5152 (1992); S. P. Tewari and G. S. Agarwal, Phys. Rev. Lett. **56**, 1811 (1986); S. E. Harris, J. E. Field, and A. Imamoglu, Phys. Rev. Lett. **64**, 1107 (1990); M. Jain, G. Y. Yin, J. E. Field, and S. E. Harris, Opt. Lett. **18**, 998 (1993).
[13] R. L. DeZafra and A. Marshall, Phys. Rev. **170**, 128 (1968).
[14] G. Y. Yin, A. Kasapi, M. Jain, and A. Merriam, in *Conference on Laser and Electro-Optics,* 1994 OSA Technical Digest Series Vol. 8 (Optical Society of America, Washington, DC, 1994), p. 118; A. Kasapi, G. Y. Yin, and M. Jain, "A Pulsed Ti:Sapphire Laser Seeded Off the Gain Peak" (to be published); T. D. Raymond, Opt. Lett. **16**, 33 (1991).
[15] D. Grischkowsky, Phys. Rev. A **7**, 2096 (1973).
[16] J. F. Reintjes, *Nonlinear Optical Parametric Processes in Liquids and Gases* (Academic Press, Orlando, FL, 1984), pp. 338–344; M. Le Berre, E. Ressayre, and A. Tallet, Phys. Rev. A **25**, 1604 (1982); Phys. Rev. A **29**, 2669 (1984); D. E. McClelland, R. J. Ballagh, and W. J. Sandle, J. Opt. Soc. Am. B **3**, 212 (1986).
[17] R. Guenther, *Modern Optics* (Wiley, New York, 1990), pp. 191–196; A. E. Siegman, *Lasers* (University Science Books, Mill Valley, CA, 1986).

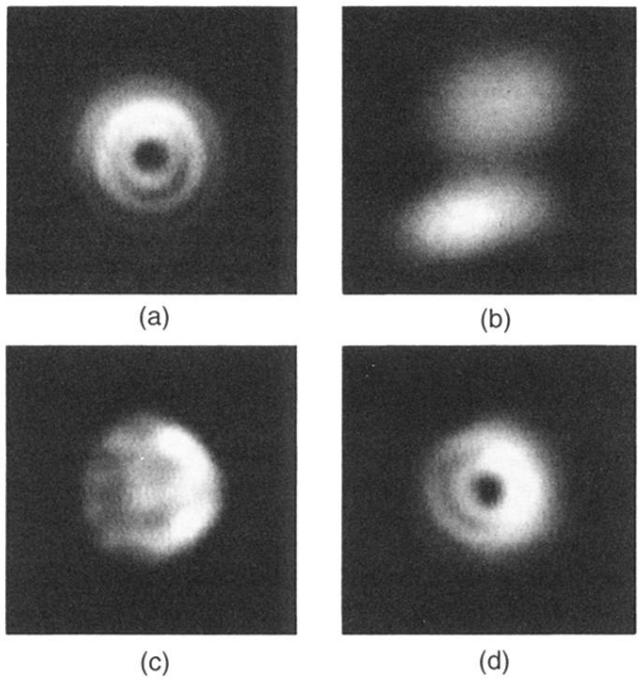

FIG. 5. Spatial images of the probe beam after passage through the Pb cell. (a) Probe alone in a cold cell (note the central dark portion and the faint diffraction rings). (b) Probe alone with a Rabi frequency of 0.5 cm^{-1} (330 kW/cm^2). Here, as in (c) and (d), $N = (1.6 \times 10^{14}) \pm 30\%$ atoms/cm^3. The figure shows a superposition of two probe pulses and is scaled to one-half size to show both images. The beam is spatially distorted and, from shot-to-shot, moves randomly by several beam diameters. (c) Probe and coupling laser with the coupling laser detuned by 200 MHz from line center ($\Omega_p = 0.3$ cm^{-1} and $\Omega_c = 0.8$ cm^{-1}). The transmitted beam is now spatially distorted. (d) Probe and coupling laser with the coupling laser at line center ($\Omega_p = 0.3$ cm^{-1} and $\Omega_c = 0.8$ cm^{-1}). The beam quality is now almost as good as in (a). In order to allow better visibility of the fringe structure, portions of these images are saturated.